American Mineralogist, Volume 92, pages 1262–1269, 2007

Crystal-chemical and carbon-isotopic characteristics of karpatite ($C_{24}H_{12}$) from the Picacho Peak Area, San Benito County, California: Evidences for the hydrothermal formation

Takuya Echigo,[1,*] Mitsuyoshi Kimata,[1] and Teruyuki Maruoka[2]

[1]Earth Evolution Sciences, Life and Environmental Sciences, University of Tsukuba, Tennoudai 1-1-1, Tsukuba 305-8572, Japan
[2]Integrative Environmental Sciences, Life and Environmental Sciences, University of Tsukuba, Tennoudai 1-1-1, Tsukuba 305-8572, Japan

Abstract

Karpatite from the Picacho Peak Area, San Benito County, California, has been characterized as an exceptionally pure crystal of coronene ($C_{24}H_{12}$) by infrared absorption analysis, Raman scattering analysis, and differential thermal analysis. Furthermore, the crystal structure of karpatite was determined using a single-crystal X-ray diffraction method for the first time. The mineral crystallizes in the monoclinic system, space group $P2_1/a$, with unit-cell dimensions of a = 16.094(9), b = 4.690(3), c = 10.049(8) Å, β = 110.79(2)°, V = 709.9(8) Å^3, and Z = 2. The structure was solved and finally refined to R_1 = 3.44% and wR_2 = 2.65%, respectively. The coronene molecules in the crystal structure of karpatite are all isolated and the intermolecular distances correspond to van der Waals interactions. The coronene molecules have the high degree of aromaticity and no overcrowded hydrogen atoms, both of which avoid a mixing of other polycyclic aromatic hydrocarbons (PAHs) in karpatite. The corrugated arrangement of coronene molecules constituting karpatite prevents intercalation reactions, accounting for the exceptional purity of this mineral.

The isotopic composition of carbon was measured, using an elemental analyzer-isotopic ratio mass spectrometer (EA/IRMS). The present karpatite yielded a $\delta^{13}C$ value of –22.39 ± 0.18‰ (vs. VPDB), which is similar to carbon isotopic compositions of sedimentary organic matter in the far-reaching tectonic regions. This organic matter might be converted to coronene molecules by hydrothermal fluids leading to formation of karpatite. Textural relationships indicate that after the strong concentration of coronene molecules in hydrothermal fluids, karpatite growth postdates both hydrothermal quartz precipitation, and subsequent cinnabar formation.

Keywords: Crystal structure, karpatite, stable isotopes, coronene, IR spectroscopy, Raman spectroscopy, DTA, polycyclic aromatic hydrocarbons

Introduction

Karpatite, previously called pendletonite or carpathite (Murdoch and Geissman 1967, 1968), was named and first described by Piotrovskii (1955) from Trans-Carpathia. The mineral was identified as a molecular crystal of coronene ($C_{24}H_{12}$, a polycyclic aromatic hydrocarbon, or PAH) on the basis of chemical analysis, melting point, UV spectrum, X-ray powder diffraction pattern, and its derived unit-cell dimensions (Murdoch and Geissman 1967). Wise et al. (1986) revealed that karpatite consists solely of coronene molecules, using high-performance liquid chromatography. In general, PAH minerals are highly complex assemblages of organic compounds that can provide insights into their genesis (Blumer 1975; Wise et al. 1986; Jehlička et al. 2006). However, karpatite is so pure that the formation process is not known at all (Wise et al. 1986).

Many structural analyses of natural karpatite and synthetic coronene were reported (natural karpatite: Frank-Kamenetskii et al. 1967; Murdoch and Geissman 1967, 1968, synthetic coronene: Robertson and White 1944, 1945; Fawcett and Trotter 1965; Krygowski et al. 1996). However, the structural refinement of natural karpatite has not been carried out. Detailed crystal-chemical analyses may provide structural insight into the perfect purity of this rare mineral, and carbon isotope analysis could trace the carbon component back to its origin in nature.

Here we present the results of infrared absorption analysis, Raman scattering analysis, the single-crystal structure analysis, and carbon isotopic analysis of karpatite from the Picacho Peak Area (San Benito County, California) in the hope of unraveling its origin and the formation process.

Samples and occurrences

Samples of karpatite were selected from specimens from the Picacho Peak Area, San Benito County, California, which is located in the New Idria District (Fig. 1). The geology of the New Idria District was studied extensively (Eckel and Meyers 1946; Coleman 1961; Linn 1968; Fox 1983; Studemeister 1984), and afterward the mineralogy of the New Idria ores has been described in detail by Boctor et al. (1987) and Dunning et al. (2005). Karpatite from the sample locality was presumed to be formed by hydrothermal activity (Murdoch and Geissman 1967).

The Picacho Peak Area is along the San Andreas Fault in

* E-mail: echigo@geol.tsukuba.ac.jp

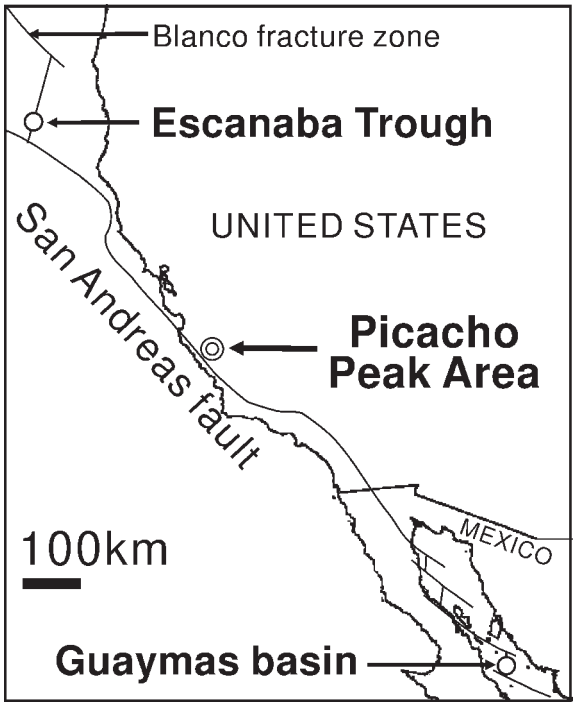

FIGURE 1. Location of the Picacho Peak Area, San Benito County, California in the West Coast. Those of Escanaba Trough and Guaymas basin are also shown.

the West Coast (Fig. 1). Hydrothermal activities associated with seafloor spreading were reviewed by Rona (1984, 1988) and Rona and Scott (1993). It was evident that hydrothermal alternation of organic matter generates PAHs such as naphthalene ($C_{10}H_8$), phenanthrene ($C_{14}H_{10}$), and coronene (Simoneit 2000). Coronene molecules were reported in the hydrothermal petroleum, occurring in the seafloor hydrothermal systems, namely Escanaba Trough (Simoneit et al. 1997) and Guaymas Basin (Simoneit and Shoell 1995). Both of them are hydrothermal vent systems at sediment-covered ridges and along the San Andreas Fault (Fig. 1).

The euhedral crystals of karpatite occur within a quartz-lined vug in a centimeter-sized quartz vein (Fig. 2), for which the host rock is a brecciated silica-carbonate rock composed principally of ferroan magnesite and quartz (Roberts et al. 1995, 2002, 2004).

ANALYTICAL METHODS

The electron microprobe observation was performed with a JSM-6320F scanning microscope (JEOL) operating with 15 kV acceleration voltage and 600 pA beam current. A back-scattered electron image was obtained to see if other minerals occurred within the boundary between the present karpatite and associated minerals.

Chemical composition of the cinnabar paragenetic with the present karpatite was analyzed qualitatively by electron microprobe analysis, which was performed with the wavelength dispersion spectroscopy (WDS) on a JEOL superprobe (JXA-8621), with a beam size of 10 μm, an acceleration voltage of 25 kV, and a beam current of 50 nA.

Single-crystal infrared spectrum was obtained to check on whether the present karpatite contains impurities or not, using a Janssen-type micro-FTIR spectrometer (JASCO corp.). A single crystal of karpatite (~20 μm thick) was chosen under a stereomicroscope and placed on a KBr plate. The spectrum was measured in the region of 2000 to 650 cm^{-1}, with 1 cm^{-1} resolution, and 500 scans were performed at room temperature in the air. The observed infrared frequencies are tabulated in Table 1.

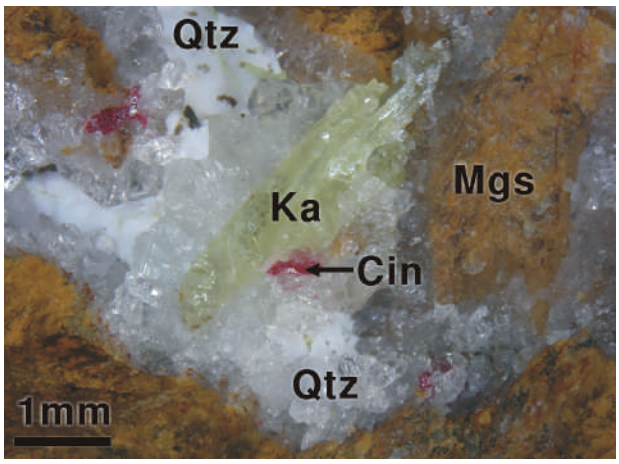

FIGURE 2. Photograph of karpatite from the Picacho Peak Area, San Benito County, California, which is crystallized on quartz containing cinnabar grains (Ka = karpatite, Qtz = quartz, Cin = cinnabar, Mgs = magnesite).

Raman scattering measurements were carried out using a micro-Raman spectrometer (Photon-Design Mars) that uses a monochromator (JOBIN YVON HR-320) and a CCD detector (ANDOR DU-401). Approximately 100 mW of power at 514.5 nm wavelength from an Ar laser (Spectra Physics Stabilite 2017) was used to excite the sample. The measurement was made in the air at room temperature.

Thermal analysis of the present karpatite was carried out with a thermogravimetric analyzer (Rigaku Thermo plus TG8120) in the air to examine the thermal behavior of the specimen. The pulverized karpatites (5.58 mg) were heated in an open platinum crucible at the rate of 10.0 °C/min up to 450 °C.

A single crystal of karpatite was chosen under a stereomicroscope and a polarizing microscope, and then a single-crystal X-ray diffraction data set was measured with an imaging-plate diffractometer system (Rigaku RAXIS-RAPID, Mo$K\alpha$ radiation, graphite monochromator). Intensity data were corrected for Lorenz and polarization effects. Empirical absorption correction (Higashi 1995) was used. Selected crystallographic and experimental data together with the refinement details are given in Table 2. Structure solution and refinement have been carried out by direct method (SIR97: Altomare et al.1999). Positions of hydrogen atoms were determined on a three-dimensional difference-Fourier map (Beurskens et al. 1999) around the associated carbon atoms. The full-matrix least-squares analyses on F^2 were done using the CRYSTALS program (Watkin et al. 1996) with anisotropic displacement parameters for carbon atoms and isotropic parameters for hydrogen atoms.

The isotopic ratio of carbon was measured, using an elemental analyzer-isotopic ratio mass spectrometer (EA/IRMS: Delta plus, Thermo Electron). The samples were weighed into tin capsules, which were introduced by an autosampler into the combustion tubing heated at 1020 °C with helium gas flowing at 100 mL/min and oxidized by a pulse of oxygen. The combustion tubing contained chromium trioxide and silvered cobaltous oxide, which promoted the complete oxidation of carbon species in the sample. The ion signals of CO_2^+ with m/z of 44, 45, and 46 were measured to determine the C isotopic compositions. The measurements were carried out six times and then mean and standard deviation were calculated.

RESULTS

Close observation on a back-scattered electron image of the present karpatite sample reveals that neither other hydrocarbons nor any other compounds were observed within the distinct boundary between karpatite and quartz (Fig. 3). An associated mineral found in the vugs is cinnabar in minuscule amounts, which is usually either anhedral or subhedral (Fig. 2). X-ray dif-

fraction (powder and single-crystal XRD) verified that the present crystals consist of only karpatite. This verification is consistent with the results of Blumer (1975) and Wise et al. (1986). In cinnabar crystals paragenetic with karpatite and quartz, the only Hg and S were detected by EMPA and other metals (e.g., Fe, Zn, and Mn) were below their detection limits of 0.1 wt%.

Three infrared absorption spectra of the present karpatite, of a synthetic crystal of pure coronene (Cyvin et al. 1982) and of isolated coronene molecules in an Ar atmosphere (Hudgins and Sandford 1998) are shown in Figure 4. In the IR spectrum of the present karpatite, 25 bands were registered and all the bands could be assigned to coronene vibrations (Table 1).

Raman scattering spectra of the present karpatite, of a synthetic crystal of pure coronene (Ying Sin et al. 2003), as well as a simulated spectrum of coronene (calculated by density functional method, Zhang and Zhang 2005) are shown in Figure 5. As well as from their infrared spectra (Fig. 4), it is evident from the Raman scattering spectra that significant contents of other hydrocarbons were not coexistent with the present karpatite.

A comparison between TG-DTA curves of the present karpatite and synthetic coronene (Martínez-Alonso et al. 1992) is shown in Figure 6. The endothermic melting peak of karpatite (432.8 °C) is nearly identical with that of synthetic coronene crystal (428 °C). There is a slight difference in TG-DTA curves between these two samples, which may be attributed to the experimental conditions: heating rate, sample weight, and the nature and flow rate of the sweeping gas (Muraishi and Suzuki 1994; Shishkin 2006). Thermal analysis of synthetic coronene was carried out in 99.995% pure Ar atmosphere at a flow rate of 50 mL/min, using 15 mg samples (Martínez-Alonso et al. 1992). The present thermal analysis also revealed that our karpatite sample contains no impurity.

The crystal structure of karpatite was finally refined to R_1 value of 3.44% (wR_2 value of 2.65%) for the 1384 unique observed [$I_o > 5\sigma(I_o)$] reflections (Table 2). The final positional parameters and displacement parameters are given in Table 3. The molecular structure of coronene in karpatite is shown in Figure 7. The carbon-carbon intramolecular bonds in the central ring are

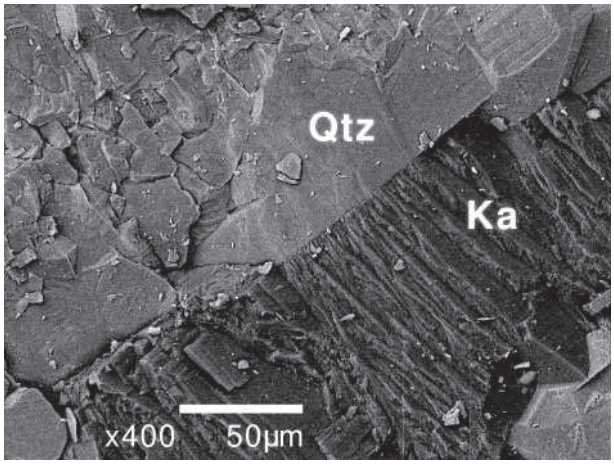

FIGURE 3. Back-scattered electron image of karpatite associated with quartz (Ka = karpatite, Qtz = quartz).

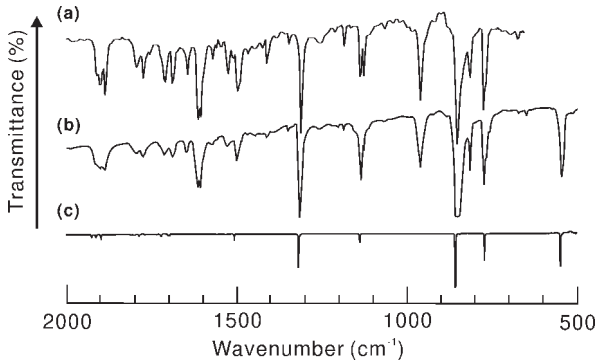

FIGURE 4. Infrared spectra of (**a**) karpatite from the Picacho Peak Area, San Benito County (this study), (**b**) synthetic crystal of coronene (Cyvin et al. 1982), and (**c**) isolated coronene molecules in argon (Hudgins and Sandford 1998).

TABLE 1. Comparison of infrared frequencies (cm^{-1}) through the aromatic C-C stretching and C-H bending regions for coronene groups

Karpatite* (this study)	Synthetic crystal of coronene†	Coronene molecules‡ (Isolated in Ar)	Interpretation
		1924.4	
1921.06	1918	1922.9	
1907.11	1904	1910.4	
1892.88	1891	1896	
1802.46	1797	1798.7	
1780.27	1777	1783.8	
		1767.6	
1716.85	1713	1718.7	
1682.74	1685	1695.5	
1653.2	1647		
1616.3	1614	1620.7	E_{1u}
1608.59	1606		
	1598		
1575.07	1575	1579.2	
		1533	
1529.74	1525	1530.4	E_{1u}
		1505.3	
1500.56	1494	1497.9	E_{1u}
1415.2	1411		
1350.09	1340		
		1318.3	
1313.68	1314	1317.4	E_{1u}
	1310		
	1297		
		1214.6	
		1210.7	
1184.92	1184		
1137.18	1133	1137	E_{1u}
1125.6	1125		E_{1u}
	962		
956.81	958		
854.57	849	857	A_{2u}
	845	846.1	A_{2u}
810.44	811		E_{1u}
769.69	769	771.6	
764.39	764		E_{1u}
	753		
668.17	646		
	549	550.5	
	544		A_{2u}
	510		
	379		E_{1u}
	151		A_{2u}
	135		

* Karpatite from San Benito County (this study).
† Infrared spectrum of coronene as KBr pellets (Cyvin et al. 1982).
‡ Infrared spectrum of matrix isolated coronene molecules in argon (Hudgins and Sandford 1998).

1.407–1.427 Å, those bonds in the "spokes" are 1.408–1.418 Å, and the two types of those bonds in outer bond are 1.349–1.356 and 1.409–1.421 Å (Fig. 7). These distances agree closely with the previous results obtained from structure refinement of the synthetic crystals (Robertson and White 1944, 1945; Fawcett and Trotter 1965; Krygowski et al. 1996), although the present karpatite is a natural crystal of coronene. The carbon-carbon intermolecular separations of less than 4 Å were calculated, and all these separations correspond to normal van der Waals interactions (Pauling 1960). The more significant distances are given in Tables 4 and 5. The C···H and H···H contacts also correspond to van der Waals interactions (Pauling 1960). The plane of the coronene molecule is inclined at approximately 45° to the **b** crystal axis, and an end view of the arrangement is schematically displayed in Figure 8a. The molecules in adjacent stacks are nearly perpendicular to each other. The distance between neighboring molecules in karpatite is 3.463 Å, which is significantly longer than interplanar distance in graphite, 3.35 Å (Fig. 8b: Hart, 1991). This elongation may be attributed to the C-H···π interaction (Lindeman et al. 1998; McKinnon et al. 2004) since the coronene molecule has hydrogen atoms though graphite only consists of carbon atoms.

Table 2. Summarized crystal data and details of refinement parameters for karpatite

Chemical formula	$C_{24}H_{12}$
Crystal dimensions	0.15 × 0.15 × 0.10 mm
Temperature	293 K
Lattice parameters	
a	16.094(9) Å
b	4.690(3) Å
c	10.049(8) Å
β	110.79(2)°
V	709.9(8) Å^3
Z	2
D_{calc}	1.407 (g/cm^3)
Space group (14)	$P2_1/a$
F000	312.00
μ (Mo*K*α)	0.799 cm^{-1}
Measured reflections	6512
Independent reflections, R_{int}	1614, 0.082
R_1, wR_2 (All data)	0.2203, 0.0624
Observed refractions [$I_o > 5\sigma(I_o)$]	1384
Parameters used in the refinement	133
Reflection/Parameter ratio	10.41
R_1 [$I_o > 5\sigma(I_o)$]	0.0344
wR_2 [$I_o > 5\sigma(I_o)$]	0.0265
Goodness of Fit Indicator	1.151
Max. peak in Final Diff. Map	0.25 e/Å^3
Min. peak in Final Diff. Map	–0.28 e/Å^3

These $\delta^{13}C$ values of the present karpatite are calculated as –22.39 ± 0.18‰ (vs. Vienna PeeDee Belemnite, VPDB), of which the carbon isotope composition is typical of coal and sedimentary organic materials of plant origin (Deines 1980; Galimov 1995).

Discussion

The mechanism of purification for karpatite

Karpatite is a natural crystalline analog of synthetic hydrocarbon coronene, which is an important, well-investigated chemical material (Szczepanski and Vala 1993; Wilcke et al. 2005). As was expected, the properties of these two materials are in good agreement with each other. It is almost impossible to distinguish karpatite from ultrapure coronene (Blumer 1975; Wise et al. 1986) by infrared absorption, Raman scattering, and differential thermal analyses (Figs. 4, 5, and 6; Table 1). The infrared frequencies of karpatite are generally lower than those

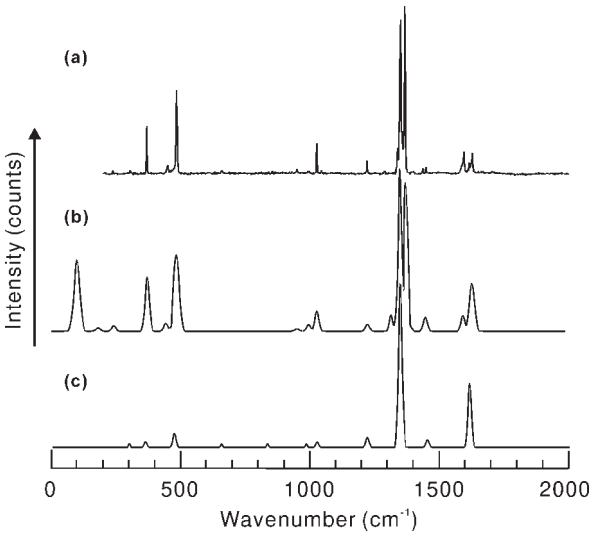

Figure 5. Raman spectra of (**a**) karpatite from the Picacho Peak Area (this study), (**b**) synthetic crystal of coronene (Ying Sin et al. 2003), and (**c**) the simulated coronene molecule by density functional method (Zhang and Zhang 2005).

Table 3. Atomic coordinates and displacement parameters (Å^2)

Atom	*x*	*y*	*z*	B_{eq}	U_{11}	U_{22}	U_{33}	U_{12}	U_{13}	U_{23}
C1	–0.11918(19)	–0.4056(6)	0.0380(3)	4.08(8)	0.049(2)	0.0492(18)	0.059(2)	0.0076(16)	0.0218(18)	0.0045(17)
C2	–0.1121(2)	–0.4800(6)	0.1771(3)	4.98(9)	0.068(2)	0.054(2)	0.080(2)	0.0075(17)	0.042(2)	0.0121(19)
C3	–0.0497(2)	–0.3620(6)	0.2925(4)	5.27(9)	0.084(2)	0.063(2)	0.068(2)	0.0182(18)	0.047(2)	0.021(2)
C4	0.01212(19)	–0.1589(6)	0.2770(3)	4.19(7)	0.068(2)	0.0505(18)	0.0452(19)	0.0178(17)	0.0256(16)	0.0068(16)
C5	0.0802(2)	–0.0347(7)	0.3949(3)	5.24(9)	0.085(2)	0.073(2)	0.039(2)	0.020(2)	0.0182(19)	0.0031(19)
C6	0.1376(2)	0.1596(7)	0.3760(3)	5.23(9)	0.071(2)	0.070(2)	0.050(2)	0.0091(19)	0.0118(19)	–0.001(2)
C7	0.13206(18)	0.2455(5)	0.2379(3)	4.09(7)	0.051(2)	0.0548(19)	0.0468(19)	0.0096(17)	0.0136(17)	–0.0004(16)
C8	0.1913(2)	0.4503(6)	0.2171(4)	5.01(9)	0.050(2)	0.058(2)	0.079(2)	0.0034(16)	0.0180(19)	–0.0107(19)
C9	0.1836(2)	0.5266(6)	0.0827(4)	4.95(8)	0.052(2)	0.054(2)	0.088(2)	–0.0014(16)	0.0319(18)	–0.004(2)
C10	–0.05971(18)	–0.2026(5)	0.0183(3)	3.42(7)	0.042(2)	0.0335(17)	0.057(2)	0.0086(15)	0.0211(18)	0.0064(16)
C11	0.0058(2)	–0.0803(6)	0.1376(2)	3.36(8)	0.0504(19)	0.0419(19)	0.044(2)	0.0133(15)	0.0273(18)	0.0077(15)
C12	0.06586(19)	0.1207(6)	0.1201(2)	3.30(8)	0.0407(18)	0.0423(18)	0.039(2)	0.0122(16)	0.0105(16)	0.0035(14)
H2	–0.1541(15)	–0.621(4)	0.190(2)	6.4(7)						
H3	–0.0462(15)	–0.410(5)	0.391(2)	7.6(7)						
H5	0.0845(16)	–0.085(5)	0.492(2)	7.5(8)						
H6	0.1858(17)	0.248(4)	0.463(3)	7.2(8)						
H8	0.2408(16)	0.530(5)	0.307(2)	8.7(8)						
H9	0.2252(13)	0.667(4)	0.069(2)	5.7(7)						

TABLE 4. Selected intermolecular bond lengths (Å) (C···C distances are listed)

Atom	Atom	Distance (Å)	Atom	Atom	Distance (Å)
C3 -	C5*	3.715(4)	C9 -	C11‡	3.607(5)
C5 -	C5†	3.885(5)	C9 -	C12‡	3.464(4)
C6 -	C3‡	3.604(4)	C9 -	C9#	3.918(5)
C7 -	C3‡	3.658(5)	C9 -	C10**	3.690(4)
C7 -	C4‡	3.496(4)	C11 -	C2‡	3.495(4)
C8 -	C4‡	3.643(4)	C12 -	C1††	3.934(4)
C8 -	C11‡	3.564(4)	C12 -	C2‡‡	3.633(5)
C8 -	C12‡	3.676(4)	C1 -	C10††	3.625(4)
C9 -	C1§	3.801(4)	C2 -	C8‡‡	3.993(5)
C9 -	C2‖	4.009(4)	C10 -	C10††	3.480(4)

Symmetry operators:
* x, y – 1, z.
† –x, –y, –z + 1.
‡ x, y + 1, z.
§ x + 1/2, –y + 1/2, z.
‖ x + 1/2, –y + 1/2 – 1, z.
–x + 1/2, y + 1/2, –z.
** –x, –y + 1, –z.
†† –x, –y – 1, –z.
‡‡ x + 1/2 – 1, –y + 1/2 – 1, z.

TABLE 5. Selected intermolecular bond lengths (Å) (C···H distances and H···H distances are listed)

Atom	Atom	Distance (Å)	Atom	Atom	Distance (Å)
H9* -	C1	2.86(2)	H6 -	H8§	2.42(3)
H9* -	C2	2.86(2)	H9 -	H2‖	2.85(3)
H9† -	C9	2.99(2)	H5 -	H3#	2.80(3)
H2‡ -	C8	3.02(2)	H5 -	H5#	2.89(3)

Symmetry operators:
* x + 1/2 – 1, –y + 1/2, z.
† –x + 1/2, y + 1/2 – 1, –z.
‡ x + 1/2, –y + 1/2 – 1, z.
§ –x + 1/2, y + 1/2 – 1, –z + 1.
‖ x + 1/2, –y + 1/2, z.
–x, –y, –z + 1.

of the isolated coronene molecules (Table 1), and this lowering may be attributed to the intermolecular interaction.

Many properties of molecular crystals are significantly influenced by those of the free molecules because of the dominance of strong intramolecular forces (Wright 1995), and thus the properties of karpatite may be derived from those of the coronene molecules. In the last few decades, the concept of aromaticity has been generally accepted (Krygowski and Cyrański 2001) as follows: aromatic compounds exhibit a tendency to retain their π-electron structure, and hence, they prefer substitution to addition. The absence of other PAHs in karpatite may be attributed to the high degree of aromaticity of coronene molecules, which was established by harmonic oscillator model of aromaticity (HOMA: Kruszewski and Krygowski 1972; Krygowski 1993; Krygowski et al. 1996; Krygowski and Cyrański 2001). For instance, idrialite consists of picene molecules ($C_{22}H_{14}$: Fig. 9a, Struntz and Contag 1965; Geissman et al. 1967), but besides, many other organic compounds are present, such as idenofluorene ($C_{20}H_{14}$: Fig. 9b) and 11H-Benzo[b]fluoreno[2,3-d]thiophene ($C_{19}H_{12}S$: Fig. 9c) (Blumer 1975; Wise et al. 1986). Picene molecules are conjugated hydrocarbon compounds and also have the high degree of aromaticity (Krygowski 1993), as well as coronene molecules in karpatite. However, picene molecules have overcrowded H atoms whose H···H distances are much shorter than the accepted van der Waals contacts (Fig. 9a). The overcrowded H atoms give rise to the intramolecular distortion (De et al. 1985), which may facilitate mixing various PAHs in idrialite. Strain-induced inclusions can occur easily, because a favorable enthalpy of mixing offsets unfavorable enthalpy caused by localized lattice strain around the impurity site (Wright 1995). Hence PAHs containing neither overcrowded H atoms nor intramolecular distortion such as indenofluorene (Fig. 9b) and 11H-Benzo[b] fluoreno[2,3-d]thiophene (Fig. 9c) can easily get mixed with the crystal structure of idrialite. In contrast, coronene molecules have neither overcrowded H atoms nor intramolecular distortions (Fig. 7), and thus the crystal structure of karpatite is characterized by densely packed, π-π stacked coronene molecules (McKinnon et al. 2004). The exceptional purity of karpatite may be attributed to the proper harmony between its crystal packing force and the molecular structure of coronene.

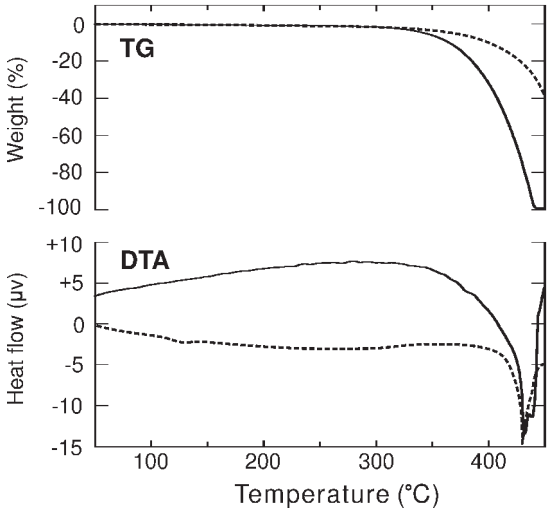

FIGURE 6. Comparison of the TG and DTA curves of the karpatite from San Benito County (solid line = this study) and synthetic crystal of coronene (dotted line = Martínez-Alomso et al. 1992).

The schematic views of crystal structures of karpatite and graphite are shown in Figures 8a and 8b, respectively, where the corrugated arrangement of coronene molecules in the former contrasts clearly with a layered structure in the latter. The distance between the hexagonal carbon layers in graphite is 3.35 Å, which corresponds to van der Waals forces (Pauling 1960). The layered structure of graphite allows many molecules and ions to be intercalated between the layers to form what are called graphite intercalation compounds (GIC: Douglas et al. 1994). Natural-GIC intercalated with ammonia molecules has been reported within graphite schist from Japan (Echigo et al. 2004). In contrast, the corrugated arrangement of coronene molecules prevents intercalation reaction in karpatite despite the fact that the molecules are held together by van der Waals forces. Although the normal distance between molecular planes of coronene in karpatite is longer than that between the layers of graphite, the corrugated structure can account for the exceptional purity of the former by the avoidance of intercalation reaction.

The origin and production process of karpatite

The carbon-isotopic compositions of coronene in hydrothermal petroleum from the Escanaba Trough (Fig. 1) are –25.6 ± 1.0‰ and –28.4‰ (vs. VPDB), indicating that the source is primarily terrestrial organic matter (Simoneit et al. 1997). On

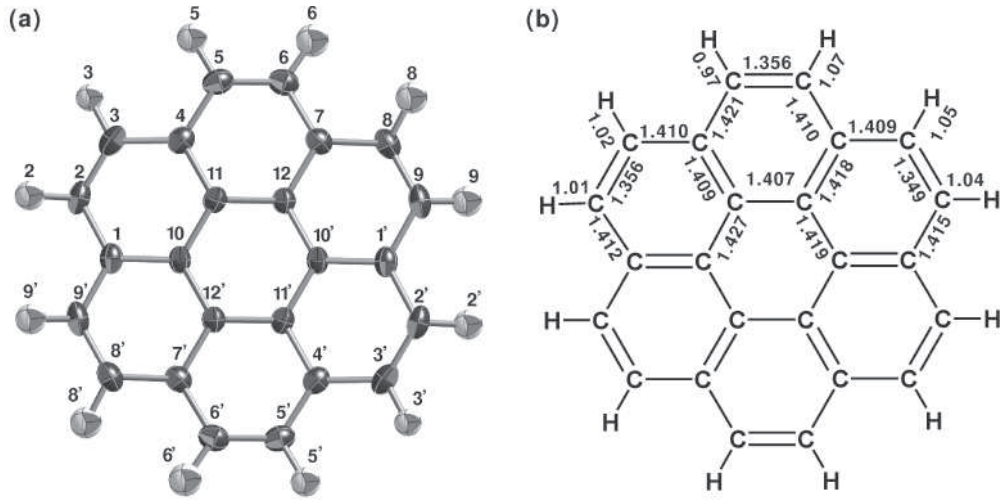

FIGURE 7. The molecular structures of coronene in karpatite. (**a**) An image of the displacement ellipsoids labeled with numbers according to Table 3. The ellipsoids, as drawn, enclose 25.0% of the probability density. Carbon and hydrogen atoms are shown as black and gray ellipsoids, respectively. (**b**) A chemical diagram based upon Kekulé structure and observed bond lengths (Å).

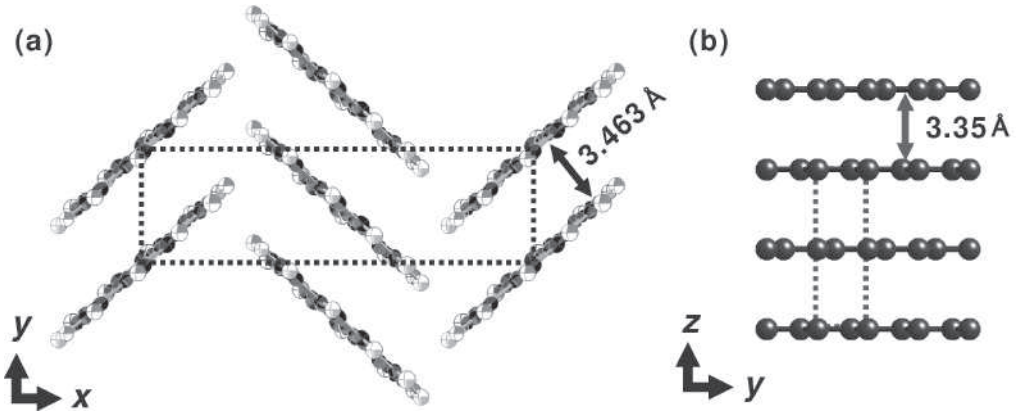

FIGURE 8. Crystal structures of (**a**) karpatite projected along [105] and (**b**) graphite projected along [100]. Carbon and hydrogen atoms are represented as black and gray spheres. Each unit cell is shown by the dotted line.

the other hand, those in the hydrothermal petroleum from the Guaymas Basin (Fig. 1) are –21.6 ± 0.9‰ and –20.1 ± 3.4‰, which reveal their marine source and confirm their generation from the sedimentary kerogen (Simoneit and Shoell 1995). The $\delta^{13}C$ values of the latter are closer to that of the present karpatite (–22.39 ± 0.18‰) than those of the former. In addition, Simoneit (2000) mentioned that hydrothermal alteration of the sedimentary kerogen yields the coronene in the produced petroleum. The Picacho Peak Area where karpatite occurred is about 30 km northeast from the San Andreas Fault (Fig. 1). Thus the $\delta^{13}C$ value and occurrence of the present karpatite may derive its origin from both sedimentary kerogen and the subsequent conversion into coronene molecules by hydrothermal fluids. An interpretation that the hydrothermal fluids led to the formation of cinnabar supports the suggestion by Studemeister (1984) that the retrograde metamorphism of Mesozoic-aged sediments released mercury-bearing fluids to form mercury-bearing minerals in the New Idria District. The sedimentary kerogen contains various organic compounds (Hayes et al. 1983), whereas karpatite consists of nearly pure coronene. The formation of karpatite must result from specific purification to avoid mixing of other PAHs.

As shown in Figure 2, the present samples provide evidence that the euhedral crystals of karpatite occurring after the crystallization of anhedral or subhedral cinnabar are crystallized on euhedral quartz. This occurrence demonstrates that the coronene molecules of karpatite were transported by hydrothermal fluids whose temperature was high enough to produce the liquid phases of both silicate and sulfide. In general, thermodynamic stability of hydrocarbons at high temperature increases with decreasing H/C-ratio, for a given carbon number (Stein 1978). Hence the PAHs of lower molecular weight such as benzene (C_6H_6), naphthalene ($C_{10}H_8$), and phenanthrene ($C_{14}H_{10}$) are depleted from high temperature fluids because of their lower thermodynamic stability. It is obvious from minerals paragenetic with the present karpatite

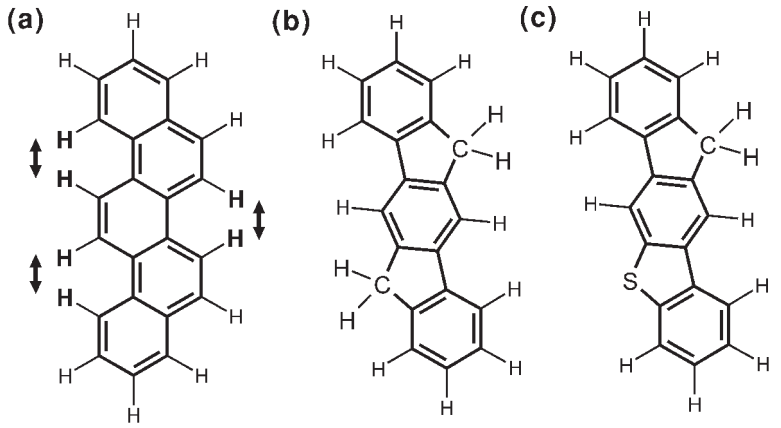

FIGURE 9. Molecular structures of (**a**) picene ($C_{22}H_{14}$), (**b**) indenofluorene ($C_{20}H_{14}$), and (**c**) 11H-Benzo[b]fluoreno[2,3-d]thiophene ($C_{19}H_{12}S$). Picene molecule has overcrowded H atoms whose H-H distances are much shorter than the accepted van der Waals contacts. Two-directional arrows show electrostatic repulsions of overcrowded H···H interactions.

that volatile PAHs had evaporated completely (Fig. 3). The PAHs of higher molecular weight had undergone each process of alternation, transportation, selective deposition/solidification, and post-depositional reworking during the hydrothermal activity (Simoneit and Fetzer 1996). Furthermore the coronene molecule is recognized as the most thermodynamically stable isomer of all $C_{24}H_{12}$ isomers (Stein and Fahr 1985). The series of reactions in nature probably leads to the concentration of coronene in the hydrothermal system and furthermore the high aromaticity of coronene might enhance the purity. In the present occurrence, karpatites are commonly crystallized on cinnabars (Fig. 2), and hence the former apparently precipitated later than the latter. In the New Idria District, cinnabar deposition was generally close to the surface at $T < 250$ °C (Studemeister 1984), and thus karpatite crystallization occurred at the lower temperature. In conclusion, the present texture of mineral aggregates indicates that after the strong concentration of coronene molecules in hydrothermal fluids, karpatite growth postdates both hydrothermal quartz precipitation and subsequent formation of cinnabar.

ACKNOWLEDGMENTS

This investigation was supported by Research Fellowships of the Japan Society for the Promotion of Science for Young Scientists (project no. 17-7332). We greatly appreciate assistance from M. Shimizu during thermal analysis and from T. Hatta during back-scattered electron microprobe experiment. Single-crystal X-ray data collection was performed at the Chemical Analysis Division, Research Facility Center for Science and Technology, University of Tsukuba. We thank T. Hama and S. Wada for providing laboratory facilities for the isotopic analysis of carbon. We are indebted to A. Kyono for useful discussion. Helpful reviews by O.V. Frank-Kamenetskaya and M. Fleck led to improvements in the manuscript.

REFERENCES CITED

Altomare, A., Burla, M., Camalli, M., Cascarano, G., Giacovazzo, C., Guagliardi, A., Moliterni, A., Polidori, G., and Spagna, R. (1999) SIR97: a new tool for crystal structure determination and refinement. Journal of Applied Crystallography, 32, 115–119.

Beurskens, P.T., Admiraal, G., Beurskens, G., Bosman, W.P., de Gelder, R., Israel, R., and Smits, J.M.M. (1999) The DIRDIF-99 program system. Technical Report of the Crystallography Laboratory, University of Nijmegen, Netherlands.

Blumer, M. (1975) Curtisite, idrialite and pendletonite, polycyclic aromatic hydrocarbon minerals: their composition and origin. Chemical Geology, 16, 245–256.

Boctor, N.Z., Shieh, Y.N., and Kullerud, G. (1987) Mercury ores from the New Idria Mining District, California: Geochemical and stable isotope studies. Geochimica et Cosmochimica Acta, 51, 1705–15.

Coleman, R.G. (1961) Jadeite deposits of the Clear Creek area, New Idria district, San Benito County, California. Journal of Petrology, 2, 209–47.

Cyvin, S.J., Cyvin, B.N., Brunvoll, J., Whitmer, J.C., and Klaeboe, P. (1982) Condensed aromatics. Part XX. Coronene. Zeitschrift für Naturforschung, Teil A: Astrophysik, Physik und Physikalische Chemie, 37A, 1359–68.

De, A., Ghosh, R., Roychowdhury, S., and Rouchowdhury, P. (1985) Structual analysis of picene, $H_{22}H_{14}$. Acta Crystallographica, C41, 907–909.

Deines, P. (1980) The isotopic composition of reduced organic carbon. In P. Fritz and J.C. Fontes, Eds., Handbook of Environmental Isotope Geochemistry, 1, The Terrestrial Environment, A, p. 329–406. Elsevier, Amsterdam.

Douglas, B.E., McDaniel, D.H., and Alexander, J.J., Eds. (1994) Concepts and models of inorganic chemistry 3rd edition, p. 928. Wiley, New York.

Dunning, G.E., Hadley, T.A., Magnasco, J., Christy, A.G., and Cooper, J.F. Jr. (2005) The Clear Creek mine, San Benito County, California: a unique mercury locality. The Mineralogical Record, 337–363.

Echigo, T., Kimata, M., Kyono, A., Takizawa, S., and Shimizu, M. (2004) Ammonia intercalated graphite from Tatarazawa, Fujioka, Japan. Japanese Magazine of Mineralogical and Petrological Sciences, 33, 77–84.

Eckel, E.B. and Meyers, W.B. (1946) Quicksilver deposits of the New Idria District, San Benito and Fresno Counties, California. California Journal of Mines and Geology, 42, 81–124.

Fawcett, J.K. and Trotter, J. (1965) The crystal structure of coronene. Proceedings of the Royal Society of London, Series A, Mathematical and physical sciences, 289, 366–376.

Fox, K.E. (1983) Malanges and their bearing on late Mesozoic and Tertiary subduction and interplane translation at the west edge of the North American plate. United States Geological Survey, Professional Paper 1198, 1–40.

Frank-Kamenetskii, V.A., Filatov, S.K., and Ya, L. (1967) Crystalline structure and chemical formula of carpathite. Mineralogicheskii Sbornik (Lvov), 21(3), 275–278.

Galimov, E.M. (1995) Fractionation of Carbon Isotopes on the Way from Living to Fossil Organic Matter. In E. Wada, T. Yonegawa, M. Minagawa, T. Ando, and B.D. Fry, Eds., Stable Isotopes in the Biosphere, p. 133–170. Kyoto University Press, Japan.

Geissman, T.A., Sim, K.Y., and Murdoch, J. (1967) Organic minerals, picene and chrysene as constituents of the mineral curtisite (idrialite). Experientia, 23, 793–794.

Hart, H. (1991) Organic Chemistry; A Short Course, 8th edition, p. 518. Houghton Milffin Company, Boston.

Hayes, J.M., Kaplan, I.R., and Wedeking, K.W. (1983) Precambrian organic geochemistry, preservation of the record. In J.W. Schopf, Ed., Origin and Evolution of the Earth's Earliest Biosphere, p. 93–134. Princeton University Press, New Jersey.

Higashi, T. (1995) Abscor—Empirical absorption correction based on Fourier series approximation. Rigaku Corporation, Tokyo.

Hudgins, D.M. and Sandford, S.A. (1998) Infrared spectroscopy of matrix isolated polycyclic aromatic hydrocarbons. 2. PAHs containing five or more rings. Journal of Physical Chemistry, 102A, 344–352.

Jehlička, J., Edwards, H.G.M., Jorge Villar, S.E., and Frank, O. (2006) Raman spectroscopic study of the complex aromatic mineral idrialite. Journal of Raman Spectroscopy, 37, 771–776.

Krygowski, T.M. (1993) Crystallographic studies of inter- and intra-molecular interactions reflected in aromatic character of σ-electron systems. Journal of Chemical Information and Computer Sciences, 33, 70–78.

Krygowski, T.M. and Cyrański, M.K. (2001) Structural aspects of aromaticity, Chemical Reviews, 101, 1385–1419.

Krygowski, T.M., Cyrański, M.K., Ciesielski, A., Świrska, B., and Leszczyński, P. (1996) Separation of the energetic and geometric contributions to aromaticity. 2. Analysis of the aromatic character of benzene rings in their various topological environments in the benzenoid hydrocarbons. Crystal and molecular structure of coronene. Journal of Chemical Information and Computer Sciences, 36, 1135–1141.

Kruszewski, J. and Krygowski, T.M. (1972) Definition of aromaticity basing on the harmonic oscillator model. Tetrahedron Letters, 13, 3839–3942.

Lindeman, S.V., Kosynkin, D., and Kochi, J.K. (1998) Unusually short (C-H···π) hydrogen bonds for effective supramolecular (aromatic/aromatic) organization in edge-to-face motifs. Journal of the American Chemical Society, 120, 13268–13269.

Linn, R.K. (1968) New Idria Mining District. In J.D. Ridge, Ed., Ore deposits of the United States, 1933–1967, p. 1624–1647. The American Institute of Mining, Metallurgical, and Petroleum Engineers, Inc., New York.

Martínez-Alonso, A., Bermejo, J., and Tascón, J.M.D. (1992) Thermoanalytical studies of pithch pyrolysis comparison with polycyclic aromatic hydrocarbons. Journal of Thermal Analysis, 38, 811–820.

McKinnon, J.J., Spackman, M.A., and Mitchell, A.S. (2004) Novel tools for visualizing and exploring intermolecular interactions in molecular crystals. Acta Crystallographica, B60, 627–668.

Muraishi, K. and Suzuki, Y. (1994) The thermal behaviour of dicarboxylic acids in various atmospheres. Thermochimica Acta, 232, 195–203.

Murdoch, J. and Geissman, T.A. (1967) Pendletonite, a new hydrocarbon mineral from California. The American Mineralogist, 52, 611–616.

——— (1968) Pendletonite: a correction. American Mineralogist, 52, 611–616.

Pauling, L. (1960) The nature of the chemical bond, 3, p. 644. Cornell University Press, New York.

Piotrovskii, G.L. (1955) Karpatite (Carpathite)-a new organic mineral from Trans-Carpathia. Mineralogicheskii Sbornik, 9, 120–127.

Roberts, A.C., Ercit, T.S., Groat. L.A., Criddle, A.J., Erd, R.C., and Williams, R.S. (1995) Peterbaylissite, $Hg_3^{1+}(CO_3)(OH)\cdot 2H_2O$, a new mineral species from the Clear Creek claim, San Benito County, California. The Canadian Mineralogist, 33, 47–53.

Roberts, A.C., Cooper, M.A., Hawthorne, F.C., Criddle, A.J., Stirling J.A.R., and Dunning, G.E. (2002) Tedhadleyite, $Hg^{2+}Hg^{1+}{}_{10}O_4I_2(Cl, Br)_2$, a new mineral species from the Clear Creek claim, San Benito County, California. The Canadian Mineralogist, 40, 909–914.

Roberts, A.C., Stirling J.A.R., Criddle, A.J., Dunning, G.E., and Spratt, J. (2004) Aurivilliusite, $Hg^{2+}Hg^{1+}OI$, a new mineral species from the Clear Creek claim, San Benito County, California, U.S.A. Mineralogical Magazine, 68, 241–245.

Robertson, J.M. and White, J.G. (1944) Crystal structure of coronene. Nature, 154, 605–606.

——— (1945) Crystal structure of coronene. Journal of the Chemical Society, 607–617.

Rona, P.A. (1984) Hydrothermal mineralization at seafloor spreading centers. Earth Science Reviews, 20, 1–104.

——— (1988) Hydrothermal mineralization at oceanic ridges. Canadian Mineralogist, 26, 431–465.

Rona, P.A. and Scott, S.D. (1993) Preface to special issue on sea-floor hydrothermal mineralization: new perspectives. Economic Geology, 88, 1933–1976.

Shishkin, Y.L. (2006) The effect of sample mass and heating rate on DSC results when studying the fractional composition and oxidative stability of lube base oils. Thermochimica Acta, 444, 26–34.

Simoneit, B.R.T. (2000) Alternation and migration of organic matter in hydrothermal systems and implications for metallogenesis. In M. Glikson and M. Mastalertz, Eds., Organic Matter and Mineralization, p. 13–37. Kluwer Academic Publishers, Great Britain.

Simoneit, B.R.T. and Fetzer J.C. (1996) High molecular weight polycyclic aromatic hydrocarbons in hydrothermal petroleums from the Gulf of California and Northeast Pacific Ocean. Organic Geochemistry, 24, 1065–1077.

Simoneit, B.R.T. and Schoell, M. (1995) Carbon isotope systematics of individual hydrocarbons in hydrothermal petroleums from the Guaymas Basin, Gulf of California. Organic Geochemistry, 23, 857–863.

Simoneit, B.R.T., Schoell, M., and Kvenvolden, K.A. (1997) Carbon isotope systematics of individual hydrocarbons in hydrothermal petroleum from Escanaba Trough, Northeastern Pacific Ocean. Organic Geochemistry, 26, 511–515.

Stein, S.E. (1978) On the high temperature chemical equilibria of polycyclic aromatic hydrocarbons. Journal of Physical Chemistry, 82, 566–571.

Stein, S.E. and Fahr, A. (1985) High-temperature stabilities of hydrocarbons. Journal of Physical Chemistry, 89, 3714–3725.

Struntz, H. and Contag, B. (1965) Evenkit, flagstaffit, idrialin und reficit. Neues Jahrbuch für Mineralogie, Monatshefte, 1, 19–25.

Studemeister, P.A. (1984) Mercury deposits of western California: an overview. Mineralium Deposita, 19, 202–207.

Szczepanski, J. and Vala, M. (1993) Infrared frequencies and intensities for astrophysically important polycyclic aromatic hydrocarbons cations. The Astrophysical Journal, 414, 646–655.

Watkin, D.J., Prout, C.K., Carruthers, J.R., and Betteridge, P.W. (1996) CRYSTALS Issue 10. Chemical Crystallography Laboratory, Oxford.

Wilcke, W., Krauss, M., Safronov, G., Fokin, A.D., and Kaupenjohann, M. (2005) Polycyclic Aromatic Hydrocarbons (PAHs) in Soils of the Moscow Region—Concentrations, Temporal Trends, and Small-Scale Distribution. Journal of Environmental Quality, 34, 1581–1590.

Wise, S.A., Campbell, R.M., West, W.R., Lee, M.L., and Bartle, K.D. (1986) Characterization of polycyclic aromatic hydrocarbon minerals, curtisite, idrialite and pendletonite using high-performance liquid chromatography, gas chromatography, mass spectrometry and nuclear magnetic resonance spectroscopy. Chemical Geology, 54, 339–357.

Wright, J.D. (1995) Molecular Crystals, 2nd edition, p. 221. Cambridge University Press, New York.

Ying Sin, S., Widjaja, E., Yu, L.E., and Garland, M. (2003) Application of FT-Raman and FTIR measurements using a novel spectral reconstruction algorithm. Journal of Raman Spectroscopy, 34, 795–805.

Zhang, D. and Zhang, R.Q. (2005) Signature of nanodiamond in Raman spectra: a density functional theoretical Study. Journal of Physical Chemistry B, 109, 9006–9013.

Manuscript received November 18, 2006
Manuscript accepted May 9, 2007
Manuscript handled by Sergey Krivovichev